ARCHIVES OF ACOUSTICS
36, 4, 795–822 (2011)
DOI: 10.2478/v10168-011-0053-5

Optimization Design of Hybrid Mufflers on Broadband Frequencies Using the Genetic Algorithm

Min-Chie CHIU

Chung Chou University of Science and Technology
Department of Mechanical and Automation Engineering
6, Lane 2, Sec. 3, Shanchiao Rd., Yuanlin
Changhua 51003, Taiwan, R.O.C.
e-mail: minchie.chiu@msa.hinet.net

(*received September 29, 2010; accepted July 22, 2011*)

Recently, there has been research on high frequency dissipative mufflers. However, research on shape optimization of hybrid mufflers that reduce broadband noise within a constrained space is sparse. In this paper, a hybrid muffler composed of a dissipative muffler and a reactive muffler within a constrained space is assessed. Using the eigenvalues and eigenfunctions, a coupling wave equation for the perforated dissipative chamber is simplified into a four-pole matrix form. To efficiently find the optimal shape within a constrained space, a four-pole matrix system used to evaluate the acoustical performance of the sound transmission loss (*STL*) is evaluated using a genetic algorithm (*GA*).

A numerical case for eliminating a broadband venting noise is also introduced. To verify the reliability of a *GA* optimization, optimal noise abatements for two pure tones (500 Hz and 800 Hz) are exemplified. Before the *GA* operation can be carried out, the accuracy of the mathematical models has been checked using experimental data. Results indicate that the maximal *STL* is precisely located at the desired target tone. The optimal result of case studies for eliminating broadband noise also reveals that the overall sound power level (*SWL*) of the hybrid muffler can be reduced from 138.9 dB(A) to 84.5 dB(A), which is superior to other mufflers (a one-chamber dissipative and a one-chamber reactive muffler). Consequently, a successful approach used for the optimal design of the hybrid mufflers within a constrained space has been demonstrated.

Keywords: dissipative, reactive, hybrid muffler, genetic algorithm, space constraints.

Notations

This paper is constructed on the basis of the following notations:

C_i – coefficients in function ($\Gamma_i = C_i e^{\gamma_i x}$),
C_o – sound speed in air (m s^{-1}),
$\widetilde{C}_o$ – sound speed in a wool (m s^{-1}),

$chrm$ – bit length of chromosome,
dh_i – the diameter of a perforated hole on the i-th inner tube (m),
D_i – diameter of the i-th perforated tubes (m),
D_o – diameter of the outer tube (m),
elt – selection of elite (1 for yes and 0 for no),
f – cyclic frequency (Hz),
gen – maximum no. of generation,
j – imaginary unit,
k – wave number for air ($= \omega/c_o$),
$\widetilde{k}(\omega)$ – the wave number for the wool,
$K(\omega)$ – the dynamic bulk modulus for a porous wool,
l_{cl} – the characteristic length,
l'_{cl} – the new characteristic length,
L_o – total length of the muffler (m),
M – mean flow Mach number,
m – face density (kg/m^2),
N_{pr} – the Prandtl number (=0.702),
OBJ – objective function (dB),
p – acoustic pressure (Pa),
pc – crossover ratio,
$\overline{p}_i$ – acoustic pressure at the i-th node (Pa),
P_0 – the pressure in atmosphere (= 101320 N/m^2),
pm – mutation ratio,
pop – no. of population,
Q – volume flow rate of venting gas (m^3 s^{-1}),
S_i – section area at the i-th node (m^2),
STL – sound transmission loss (dB),
$SWLO$ – unsilenced sound power level inside the muffler's inlet (dB),
SWL_T – overall sound power level inside the muffler's outlet (dB),
t_i – the thickness of the i-th inner perforated tube (m),
TS_{ij} – components of four-pole transfer matrices for an acoustical mechanism with straight ducts,
TPD_{ij} – components of a four-pole transfer matrix for an acoustical mechanism with a perforated chamber filled with sound absorbing wool,
$TSEC$ – components of four-pole transfer matrices for contracted part of an extended duct,
$TSEE$ – components of four-pole transfer matrices for expanded part of an extended duct,
T^*_{ij} – components of a four-pole transfer system matrix,
$\overline{u}_i$ – acoustic particle velocity at the i-th node (m s^{-1}),
u – acoustical particle velocity passing through a perforated hole from the i-th node to the j-th node (m s^{-1}),
V_1 – mean flow velocity at the inner perforated tube (m s^{-1}),
V_2 – mean flow velocity at the outer tube (m s^{-1}),
ρ_o – air density (kg m^{-3}),
$\widetilde{\rho}_o$ – wool density (kg m^{-3}),

ρ_i – acoustical density at the i-th node,
ς_i – specific acoustical impedance of the i-th inner perforated tube,
η_i – the porosity of the i-th inner perforated tube,
α_∞ – the structure factor for the wool,
Ω – the porosity for the wool,
σ_{fr} – the flowing resistance for the wool,
r_i – i-th eigen value of $[\mathrm{N}]_{4\times4}$,
γ – specific heat ratio of air (=1.4),
μ – viscosity for the air($=1.84\cdot10^{-5}\mathrm{kgm^{-1}s^{-1}}$),
ω – angular velocity ($=2\pi f$),
$[\Omega]_{4\times4}$ – the model matrix formed by four sets of eigen vectors $\Omega_{4\times1}$ of $[\mathrm{N}]_{4\times4}$.

1. Introduction

Research on mufflers that reduce high frequency noise using a duct lined with sound absorbing material was initiated by Morse (1939). Scott (1946) used a volume model for solving the acoustical performance of both the circular and rectangular duct lined mufflers with porous material. Ko (1975) assessed the sound transmission loss in acoustically lined flow ducts separated by porous splitters. Cummings and Chang (1987) investigated the duct's acoustical performance at various mean flows using the characteristics of bulk-reacting liners in circular ducts. On the basis of infinite ducts, the above research was an analysis of the acoustical performance of the duct at a fixed diameter. Cummings and Chang (1988) developed a modal method for analyzing a dissipative flow duct silencer of finite length with internal mean flow in the absorbent material. Glav (2000) extended his previous work (null-field and mode-matching) to dissipative silencers of finite length with arbitrary cross-sectional areas using a transfer matrix method. Concerning the volume modulus, Peat (1991) used a transfer matrix in evaluating the acoustical performance for an absorbing silencer element. Selamet *et al.* (2001, 2003) assessed the acoustical attenuation for perforated concentric absorbing silencers and hybrid silencers using a one-dimensional analytical method, a three-dimensional boundary element method (BEM), and an experimental study. Wang (1992) proposed a three-dimensional boundary element method (BEM) for analyzing the acoustical performance of a one-chamber dissipative muffler. Regarding plane wave theory, Munjal (2003) proposed a four-pole transfer matrix in solving the sound attenuation of pod silencers lined with porous material. Xu *et al.* (2004) assessed the sound attenuation in dissipative expansion chambers using the characteristic equation. However, the assessment of a muffler's optimal shape design within a constrained space was ignored.

In 1978, an assessment of a perforated acoustical element used to depress low frequency sound energy was introduced and discussed by Sullivan, Crocker (1978). On the basis of coupled differential equations, a series of theoretical

and numerical techniques in decoupling the acoustical problems have been proposed (Sullivan, 1979a, 1979b; Thawani, Jayaraman, 1983; Rao, Munjal, 1984; Jayaraman, Yam, 1981; Munjal *et al.*, 1987). Peat (1988) publicized a successful numerical decoupling method by finding the eigen value in transfer matrices. Previously (Chiu *et al.*, 2008), shape optimization of one-chamber mufflers equipped with a perforated resonating tube within a constrained space has been discussed. However, its acoustical performance was insufficient when dealing with a higher and broader frequency noise because of the characteristic narrow band effect. Therefore, to improve acoustical efficiency, an assessment of hybrid mufflers composed of a dissipative muffler (a one-chamber perforated chamber lined with porous material) and a one-chamber reactive muffler (a one-chamber muffler with internal extended tube) is presented. To access the acoustical property of porous material (ie., flowing resistance for a porous wool) for the dissipative muffler, the dynamic bulk modulus expression deduced by Allard, Champoux (1992) and Johnson *et al.* (1987) has been adopted. Here, the numerical decoupling methods used in forming a four-pole system matrix are in line with the genetic algorithm (*GA*) method. These, in turn, are responsible for developing a new muffler shape by adjusting the geometric parameters and the acoustical property of the wool within certain space constraints.

2. Theoretical background

In this paper, the reactive/dissipative/hybrid mufflers were adopted for noise abatement in the space-constrained root blower system shown in Fig. 1. The outlines for these mufflers as noise-reduction devices are shown in Fig. 2. The recognition of acoustical elements and the related acoustic pressure p and acous-

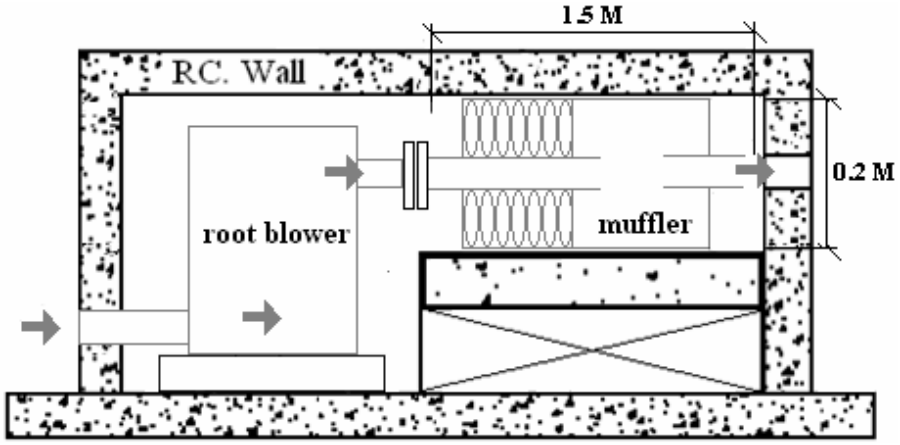

Fig. 1. The space-constrained root blower room.

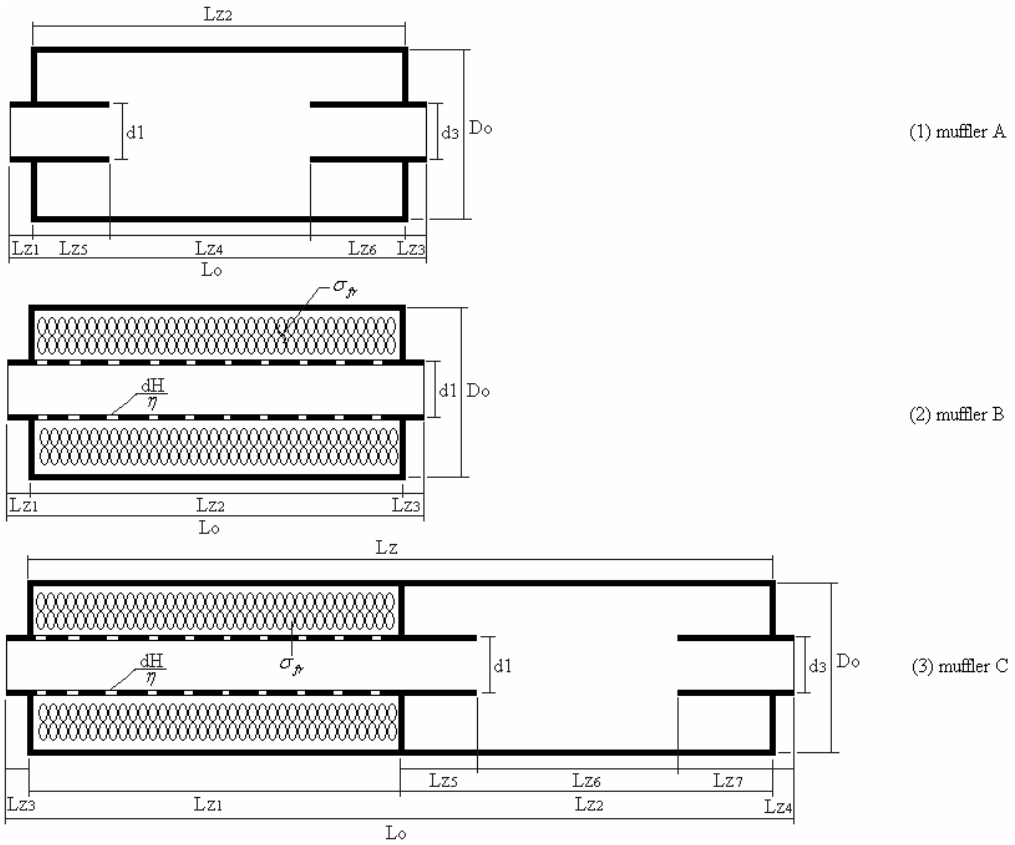

Fig. 2. The outlines of three kinds of mufflers (muffler A: one-chamber muffler with internal extended tubes; muffler B: one-chamber dissipative muffler; muffler C: two-chamber hybrid muffler).

tic particle velocity u for various mufflers is depicted in Fig. 3. As indicated in Fig. 3A, the one-chamber reactive muffler (muffler A) composed of five acoustical elements is identified as having three categories of components – three straight ducts (I), one expanded part of an extended tube (II), and one contracted part of an extended tube (III). Figure 3B indicates that the one-chamber dissipative muffler (muffler B) composed of three acoustical elements is identified as having two categories of components – two straight ducts (I), and one perforated chamber filled with porous sound absorbing material (II). Figure 3C indicates that the two-chamber hybrid muffler (muffler C) composed of seven acoustical elements is identified as having four categories of components – four straight ducts (I), and one perforated chamber filled with porous sound absorbing material (II), one expanded part of an extended tube (III), and one contracted part of an extended tube (IV). The detailed mathematical derivation of various muffler systems is presented below.

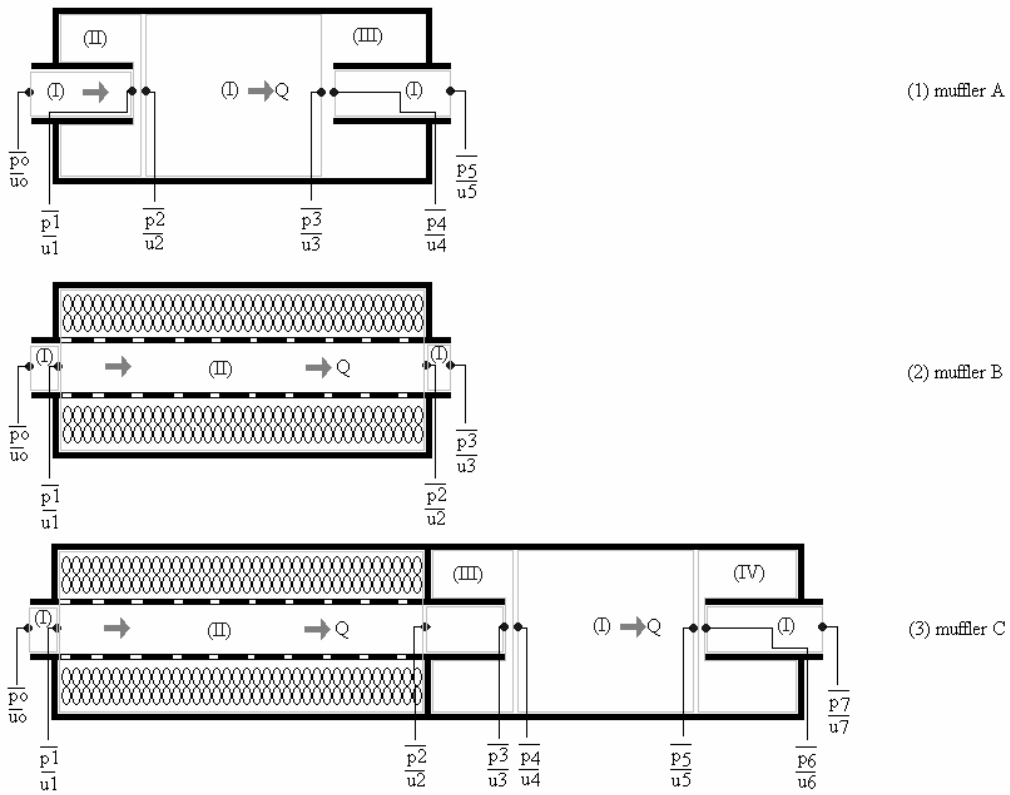

Fig. 3. The recognition of acoustical elements and the related acoustic pressure p and acoustic particle velocity u for various mufflers A–C.

2.1. A one-chamber reactive muffler (muffler A)

As derived in a previous paper (Chiu, 2009), individual transfer matrices with respect to straight ducts and an internal expanded/contracted extended tube are described as follows:

$$\begin{pmatrix} \overline{p}_0 \\ \rho_o c_o \overline{u}_0 \end{pmatrix} = e^{-jM_1 k(L_{Z1}+L_{Z5})/(1-M_1^2)} \begin{bmatrix} TS11_{1,1} & TS11_{1,2} \\ TS11_{2,1} & TS11_{2,2} \end{bmatrix} \begin{pmatrix} \overline{p}_1 \\ \rho_o c_o \overline{u}_1 \end{pmatrix}, \quad (1)$$

$$\begin{pmatrix} \overline{p}_1 \\ \rho_o c_o \overline{u}_1 \end{pmatrix} = \begin{bmatrix} TSEE12_{1,1} & TSEE12_{1,2} \\ TSEE12_{2,1} & TSEE12_{2,2} \end{bmatrix} \begin{pmatrix} \overline{p}_2 \\ \rho_o c_o \overline{u}_2 \end{pmatrix}, \quad (2)$$

$$\begin{pmatrix} \overline{p}_2 \\ \rho_o c_o \overline{u}_2 \end{pmatrix} = e^{-jM_2 k L_{Z4}/(1-M_2^2)} \begin{bmatrix} TS13_{1,1} & TS13_{1,2} \\ TS13_{2,1} & TS13_{2,2} \end{bmatrix} \begin{pmatrix} \overline{p}_3 \\ \rho_o c_o \overline{u}_3 \end{pmatrix}, \quad (3)$$

$$\begin{pmatrix} \overline{p}_3 \\ \rho_o c_o \overline{u}_3 \end{pmatrix} = \begin{bmatrix} TSEC14_{1,1} & TSEC14_{1,2} \\ TSEC14_{2,1} & TSEC14_{2,2} \end{bmatrix} \begin{pmatrix} \overline{p}_4 \\ \rho_o c_o \overline{u}_4 \end{pmatrix}, \quad (4)$$

$$\begin{pmatrix} \overline{p}_4 \\ \rho_o c_o \overline{u}_4 \end{pmatrix} = e^{-jM_4 k(L_{Z3}+L_{Z6})/(1-M_4^2)} \begin{bmatrix} TS15_{1,1} & TS15_{1,2} \\ TS15_{2,1} & TS15_{2,2} \end{bmatrix} \begin{pmatrix} \overline{p}_5 \\ \rho_o c_o \overline{u}_5 \end{pmatrix}. \quad (5)$$

The total transfer matrix assembled by multiplication is

$$\begin{Bmatrix} \overline{p}_0 \\ \rho_o c_o \overline{u}_0 \end{Bmatrix} = \prod_m [T_m(f)] \begin{Bmatrix} \overline{p}_5 \\ \rho_o c_o \overline{u}_5 \end{Bmatrix}. \quad (6)$$

The sound transmission loss (STL) of muffler A is expressed as (Munjal, 1987)

$$STL(Q, f, RT_1^*, RT_2^*, RT_3^*, RT_4^*) = 20 \log \left(\frac{1}{2}(T_{11} + T_{12} + T_{21} + T_{22}) \right) + 10 \log (S_1/S_5), \quad (7)_1$$

where

$$RT_1^* = L_{Z2}/L_{Z0}; \qquad RT_2^* = L_{Z4}/L_{Z2}; \qquad RT_3^* = d_1/D_o; \qquad RT_4^* = d_3/D_o. \quad (7)_2$$

2.2. A one-chamber dissipative muffler (muffler B)

As shown in Appendix, the transfer matrix of a perforated chamber filled with sound absorbing wool is derived. The individual matrixes with respect to straight ducts and a perforated resonating tube are described as follows:

$$\begin{pmatrix} \overline{p}_1 \\ \rho_o c_o \overline{u}_1 \end{pmatrix} = e^{-jM_1 k L_1/(1-M_1^2)} \begin{bmatrix} TS21_{1,1} & TS21_{1,2} \\ TS21_{2,1} & TS21_{2,2} \end{bmatrix} \begin{pmatrix} \overline{p}_2 \\ \rho_o c_o \overline{u}_2 \end{pmatrix}, \quad (8)$$

$$\begin{pmatrix} \overline{p}_2 \\ \rho_o c_o \overline{u}_2 \end{pmatrix} = \begin{bmatrix} TPD22_{1,1} & TPD22_{1,2} \\ TPD22_{2,1} & TPD22_{2,2} \end{bmatrix} \begin{pmatrix} \overline{p}_3 \\ \rho_o c_o \overline{u}_3 \end{pmatrix}, \quad (9)$$

$$\begin{pmatrix} \overline{p}_3 \\ \rho_o c_o \overline{u}_3 \end{pmatrix} = e^{-jM_1 k L_3/(1-M_1^2)} \begin{bmatrix} TS23_{1,1} & TS23_{1,2} \\ TS23_{2,1} & TS23_{2,2} \end{bmatrix} \begin{pmatrix} \overline{p}_4 \\ \rho_o c_o \overline{u}_4 \end{pmatrix}. \quad (10)$$

The total transfer matrix assembled by multiplication is

$$\begin{Bmatrix} \overline{p}_1 \\ \rho_o c_o \overline{u}_1 \end{Bmatrix} = \prod_m [T_m(f)] \begin{Bmatrix} \overline{p}_4 \\ \rho_o c_o \overline{u}_4 \end{Bmatrix} \quad (11)$$

The sound transmission loss (STL) of muffler A is expressed as (Munjal, 1987)

$$STL(Q, f, RT_1^{**}, RT_2^{**}, RT_3^{**}, RT_4^{**}, RT_5^{**}) = 20 \log \left(\frac{1}{2}(T_{11} + T_{12} + T_{21} + T_{22}) \right) + 10 \log (S_1/S_4), \quad (12)_1$$

where

$$RT_1^{**} = L_2/L_o; \qquad RT_2^{**} = \sigma_{fr}; \qquad RT_3^{**} = d\mathrm{H};$$
$$RT_4^{**} = \eta; \qquad RT_5^{**} = d_1/D_o. \tag{12}_2$$

2.3. A two-chamber hybrid muffler (muffler C)

Similarly, the individual matrixes with respect to various acoustical elements are described as follows:

$$\begin{pmatrix} \overline{p}_1 \\ \rho_o c_o \overline{u}_1 \end{pmatrix} = e^{-jM_1 kL_1/(1-M_1^2)} \begin{bmatrix} TS31_{1,1} & TS31_{1,2} \\ TS31_{2,1} & TS31_{2,2} \end{bmatrix} \begin{pmatrix} \overline{p}_2 \\ \rho_o c_o \overline{u}_2 \end{pmatrix}, \tag{13}$$

$$\begin{pmatrix} \overline{p}_2 \\ \rho_o c_o \overline{u}_2 \end{pmatrix} = \begin{bmatrix} TPD32_{1,1} & TPD32_{1,2} \\ TPD32_{2,1} & TPD32_{2,2} \end{bmatrix} \begin{pmatrix} \overline{p}_3 \\ \rho_o c_o \overline{u}_3 \end{pmatrix}, \tag{14}$$

$$\begin{pmatrix} \overline{p}_3 \\ \rho_o c_o \overline{u}_3 \end{pmatrix} = e^{-jM_3 kL_{Z5}/(1-M_3^2)} \begin{bmatrix} TS33_{1,1} & TS33_{1,2} \\ TS33_{2,1} & TS33_{2,2} \end{bmatrix} \begin{pmatrix} \overline{p}_4 \\ \rho_o c_o \overline{u}_4 \end{pmatrix}, \tag{15}$$

$$\begin{pmatrix} \overline{p}_4 \\ \rho_o c_o \overline{u}_4 \end{pmatrix} = \begin{bmatrix} TSEE34_{1,1} & TSEE34_{1,2} \\ TSEE34_{2,1} & TSEE34_{2,2} \end{bmatrix} \begin{pmatrix} \overline{p}_5 \\ \rho_o c_o \overline{u}_5 \end{pmatrix}, \tag{16}$$

$$\begin{pmatrix} \overline{p}_5 \\ \rho_o c_o \overline{u}_5 \end{pmatrix} = e^{-jM_5 kL_{Z6}/(1-M_5^2)} \begin{bmatrix} TS35_{1,1} & TS35_{1,2} \\ TS35_{2,1} & TS35_{2,2} \end{bmatrix} \begin{pmatrix} \overline{p}_6 \\ \rho_o c_o \overline{u}_6 \end{pmatrix}, \tag{17}$$

$$\begin{pmatrix} \overline{p}_6 \\ \rho_o c_o \overline{u}_6 \end{pmatrix} = \begin{bmatrix} TSEC36_{1,1} & TSEC36_{1,2} \\ TSEC36_{2,1} & TSEC36_{2,2} \end{bmatrix} \begin{pmatrix} \overline{p}_7 \\ \rho_o c_o \overline{u}_7 \end{pmatrix}, \tag{18}$$

$$\begin{pmatrix} \overline{p}_7 \\ \rho_o c_o \overline{u}_7 \end{pmatrix} = e^{-jM_7 k(L_{Z4}+L_{Z7})/(1-M_7^2)} \begin{bmatrix} TS37_{1,1} & TS37_{1,2} \\ TS37_{2,1} & TS37_{2,2} \end{bmatrix} \begin{pmatrix} \overline{p}_8 \\ \rho_o c_o \overline{u}_8 \end{pmatrix}. \tag{19}$$

The total transfer matrix assembled by multiplication is

$$\begin{Bmatrix} \overline{p}_1 \\ \rho_o c_o \overline{u}_1 \end{Bmatrix} = \prod_m [T_m(f)] \begin{Bmatrix} \overline{p}_8 \\ \rho_o c_o \overline{u}_8 \end{Bmatrix} \tag{20}$$

The sound transmission loss (STL) of muffler A is expressed as (Munjal, 1987)

$$STL(Q, f, RT_1, RT_2, RT_3, RT_4, RT_5, RT_6, RT_7, RT_8)$$
$$= 20\log\left(\frac{1}{2}(T_{11} + T_{12} + T_{21} + T_{22})\right) + 10\log\left(S_1/S_8\right), \tag{21}_1$$

where

$$RT_1 = L_Z/L_o; \qquad RT_2 = L_{Z1}/L_Z; \qquad RT_3 = L_{Z6}/L_{Z2};$$
$$RT_4 = D_1/D_o; \qquad RT_5 = D_3/D_o; \qquad RT_6 = \sigma_{fr}; \tag{21}_2$$
$$RT_7 = \eta; \qquad RT_8 = \mathrm{dH}.$$

2.4. Overall sound power level

The overall SWL_{T} silenced by the muffler at the outlet is

$$SWL_{\mathrm{T}} = 10\log_{10}\left(\sum_m 10^{(SWL(f_m)-STL(f_m))/10}\right), \tag{22}$$

where (1) $SWL(f_m)$ is the original SWL at the inlet of the muffler (or pipe outlet), and m is the index of the octave band frequency; (2) $STL(f_m)$ is the muffler's STL with respect to the relative octave band frequency.

2.5. Objective function

By using the formulas of Eqs. (7), (12) and (21), the objective function used in the *GA* optimization with respect to each type of muffler was established. For muffler A, the objective function in maximizing the STL at the pure tone (f) is

$$OBJ_{11} = STL(f, RT_1^*, RT_2^*, RT_3^*, RT_4^*). \tag{23}$$

The objective function in eliminating the overall SWL_{T} is

$$OBJ_{12} = SWL_{\mathrm{T}}(RT_1^*, RT_2^*, RT_3^*, RT_4^*). \tag{24}$$

Similarly, for muffler B, the objective function in maximizing the STL at the pure tone (f) is

$$OBJ_{21} = STL(f, RT_1^{**}, RT_2^{**}, RT_3^{**}, RT_4^{**}, RT_5^{**}). \tag{25}$$

The objective function in eliminating the overall SWL_{T} is

$$OBJ_{22} = SWL_{\mathrm{T}}(RT_1^{**}, RT_2^{**}, RT_3^{**}, RT_4^{**}, RT_5^{**}). \tag{26}$$

Likewise, for muffler C, the objective function in maximizing the STL at the pure tone (f) is

$$OBJ_{31} = STL(f, RT_1, RT_2, RT_3, RT_4, RT_5, RT_6, RT_7, RT_8). \tag{27}$$

The objective function in eliminating the overall SWL_{T} is

$$OBJ_{32} = SWL_{\mathrm{T}}(RT_1, RT_2, RT_3, RT_4, RT_5, RT_6, RT_7, RT_8). \tag{28}$$

3. Model check

Before performing the *GA* optimal simulation on the mufflers, an accuracy check of the mathematical model on the acoustical elements of muffler A and muffler B are performed using the experimental data from Wang, Hsieh (2000) and Lee (2005). As depicted in Figs. 4 and 5, the theoretical and experimental data are in agreement. Therefore, the proposed fundamental mathematical models are acceptable. Consequently, the model linked with the numerical method is applied to the shape optimization in the following section.

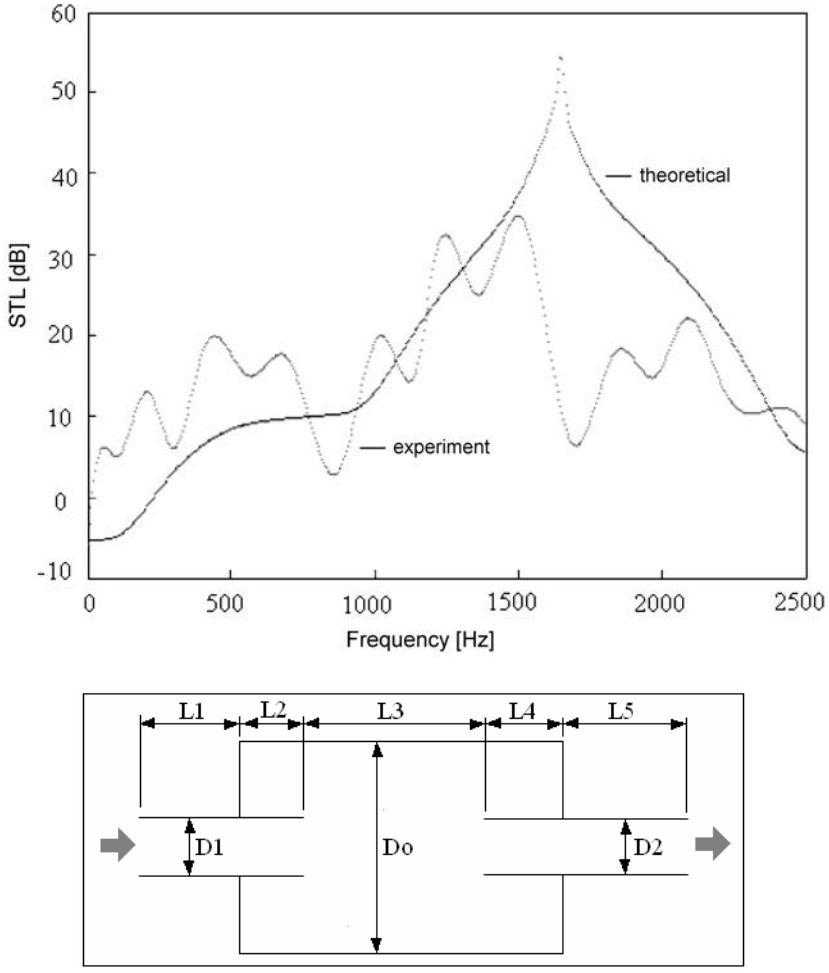

Fig. 4. Performance of a single-chamber muffler with extended tubes at the mean flow velocity of 3.4 m/sec [$D_1 = D_2 = 0.0365$ (m); $D_o = 0.108$ (m); $L_1 = L_5 = 0.1$ (m); $L_2 = L_4 = 0.052$ (m); $L_3 = 0.104$ (m)]. [Experiment data is from Wang and Hsieh (2000)].

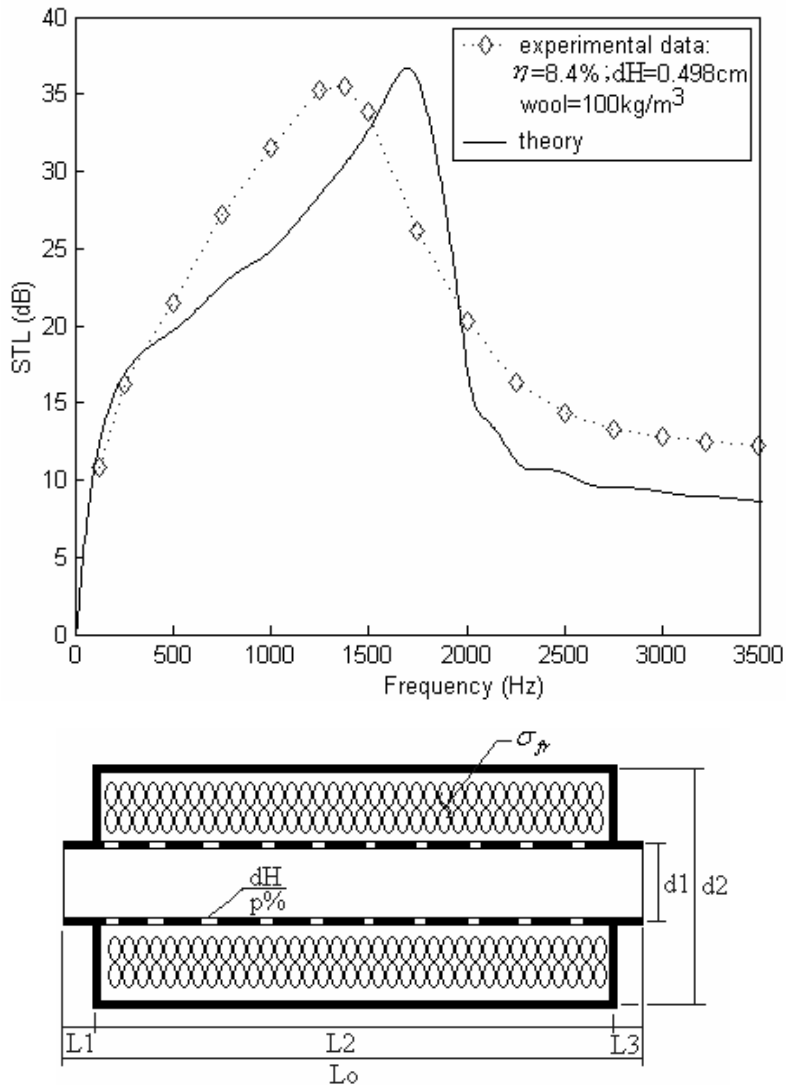

Fig. 5. Performance of a single-chamber dissipative muffler without the mean flow [$L = 0.2572$ (m); $d1 = 0.049$ (m); $d2 = 0.1644$ (m); $\eta = 8.4\%$; $dH = 0.00498$ (m); density = 100 (kg/m^3); $M = 0$]. [Experimental data is from Lee (2005)].

4. Case study

In this paper, a muffler confined inside a root blower system is shown in Fig. 1. The primary blower's sound power level inside the pipe outlet (muffler's inlet) is listed in Table 1. To efficiently reduce the sound energy, three kinds of mufflers (mufflers A–C) are adopted. As shown in Figs. 1 and 2, the available space for a cylindrical muffler is 0.2 m in diameter, and 1.5 m in length.

Table 1. Unsilenced *SWL* of a root blower inside a duct outlet.

f [Hz]	125	250	500	1000	overall
SWLO [dB(A)]	125	132	137	130	138.9

On the basis of the plane wave theory, the diametrical cut-off frequency $\left(f_c = \dfrac{1.84c}{\pi d}(1-M^2)^{0.5}\right)$ is 1005 Hz; therefore, a frequency with 1000 Hz is considered. To simplify the optimization, the flow rate ($Q = 0.02$ (m^3/s)) and the thickness of the inner tube ($t = 0.0015$ (m)) are preset in advance. The proposed material for the muffler's shell is carbon steel. The thickness of the shell is 10 mm. According to the mass law ($STL = 20\log(\mathrm{mf})$), the shell's approximate STL with respect to 125–1000 Hz are 32–50 dB. The wall resonance calculated by $f_c = \dfrac{c^2}{2\pi t}\left(\dfrac{12\rho}{E}\right)^{0.5}$ will be 1267 Hz. In order to reduce the influence of the noise emitted from the shell, the shell of the muffler will be wrapped in a cladding material (one layer of sound absorbing material).

The corresponding space constraints and the ranges of design parameters are summarized in Table 2. Before the minimization of the broadband noise is performed, the maximization of the STL at the targeted pure tones (500 Hz and 800 Hz) is performed for the purpose of an accuracy check on the GA method.

Table 2. The corresponding space constraints and the ranges of the design parameters for mufflers.

	Range of design parameters
Muffler A	$Q = 0.02$ (m^3/s) ; $L_o = 1.5$ (m); $D_o = 0.2$ (m); RT_1^*–RT_4^*:[0.2, 0.8]
Muffler B	$Q = 0.02$ (m^3/s); $L_o = 1.5$ (m); $D_o = 0.2$ (m); RT_1^{**}:[0.2, 0.8]; RT_2^{**}:[4000, 12000]; RT_3^{**}:[0.00175, 0.007]; RT_4^{**}:[0. 03, 0.1]; RT_5^{**}:[0.4, 0.8]
Muffler C	$Q = 0.02$ (m^3/s) ; $L_o = 1.5$ (m); $D_o = 0.2$ (m); RT_1: [0.4, 0.8]; RT_2–RT_5:[0.2, 0.8]; RT_6:[4000, 12000]; RT_7:[0. 00175, 0.007]; RT_8:[0.03, 0.1]
Note:	
(1) Muffler A:	$RT_1^* = L_{Z2}/L_o$; $RT_2^* = L_{Z4}/L_{Z2}$; $RT_3^* = d_1/D_o$; $RT_4^* = d_3/D_o$
(2) Muffler B:	$RT_1^{**} = L_2/L_o$; $RT_2^{**} = \sigma_{fr}$; $RT_3^{**} = d\mathrm{H}$; $RT_4^{**} = \eta$; $RT_5^{**} = d_1/D_o$
(3) Muffler C:	$RT_1 = L_Z/L_o$; $RT_2 = L_{Z1}/L_Z$; $RT_3 = L_{Z6}/L_{Z2}$; $RT_4 = d_1/D_o$; $RT_5 = d_3/D_o$; $RT_6 = \sigma_{fr}$; $RT_7 = d\mathrm{H}$; $RT_8 = \eta$

5. GA optimization

The concept of Genetic Algorithms, first formalized by HOLLAND (1975) and later extended to functional optimization by JONG (1975), involves the use of optimization search strategies patterned after the Darwinian notion of natural selection and evolution. During a *GA* optimization, one set of trial solutions was chosen and "evolved" toward an optimal solution.

For the optimization of the objective function (OBJ), the design parameters of $(X_1, X_2, \ldots, X_k)$ were determined. Because *chrm* (the bit length of the chromosome) was first chosen, the interval of the design parameter (X_k) with $[Lb, Ub]_k$ was then mapped to the band of the binary value. The mapping system between the variable interval of $[Lb, Ub]_k$ and the k-th binary chromosome of

$$[\underbrace{0\ 0\ 0\ 0\ \bullet\ \bullet\ \bullet\ 0\ 0\ 0}_{chrm} \sim \underbrace{1\ 1\ 1\ 1\ \bullet\ \bullet\ \bullet\ 1\ 1\ 1}_{chrm}$$

was subsequently built. The encoding from x to $B2D$ (binary to decimal) can be performed as

$$B2D_k = \text{integer}\left\{\frac{x_k - Lb_k}{Ub_k - Lb_k}(2^{chrm} - 1)\right\}. \tag{29}$$

The initial population was built up by randomization. The parameter set was encoded to form a string, which represented the chromosome. By evaluating the objective function (OBJ), the whole chromosome set of $[B2D_1, B2D_2, \ldots, B2D_k]$ that changed from binary form to decimal form was assigned a fitness by decoding the transformation system individually

$$\text{fitness} = OBJ(X_1, X_2, \ldots, X_k), \tag{30}_1$$

where

$$X_k = B2D_k * (Ub_k - Lb_k)/(2^{chrm} - 1) + Lb_k. \tag{30}_2$$

To process the elitism of a gene, the tournament selection, a random comparison of the relative fitness from pairs of chromosome, was adopted.

During the *GA* optimization, one pair of offspring was generated from the selected parent by a uniform crossover with a probability of *pc*. Genetically, mutation occurred with a probability of *pm* by which the new and unexpected point was brought into the *GA* optimizer's search domain. To prevent the best gene from disappearing and to improve the accuracy of optimization during reproduction, the elitism scheme, keeping the best gene (one pair) in the parent generation with a tournament strategy in a gene pool, was presented and developed. The operations in the *GA* method are depicted in Fig. 6. The process was terminated when the number of generations exceeded a pre-selected value of *gen*. The block diagram of the *GA* optimization on mufflers is depicted in Fig. 7.

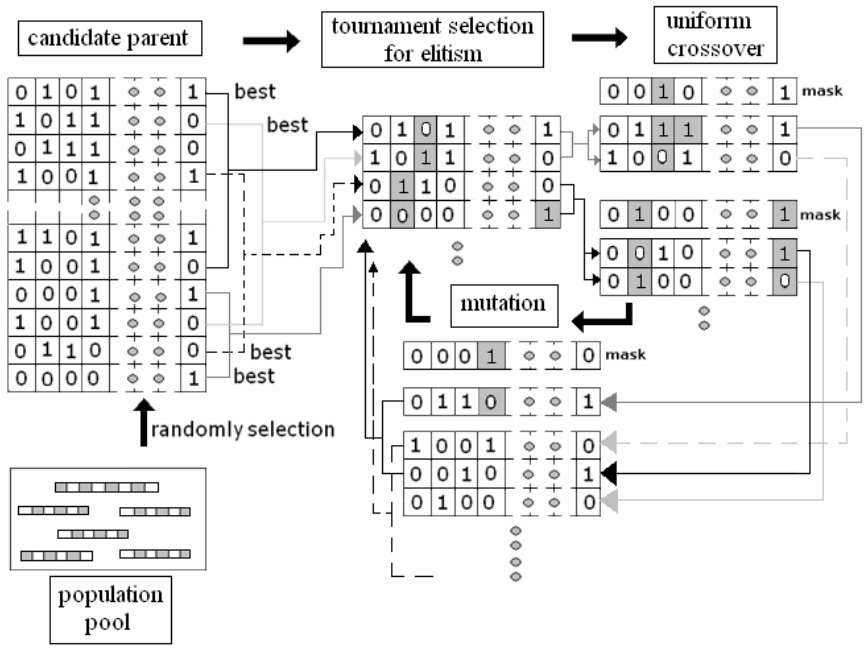

Fig. 6. Operations in the *GA* method.

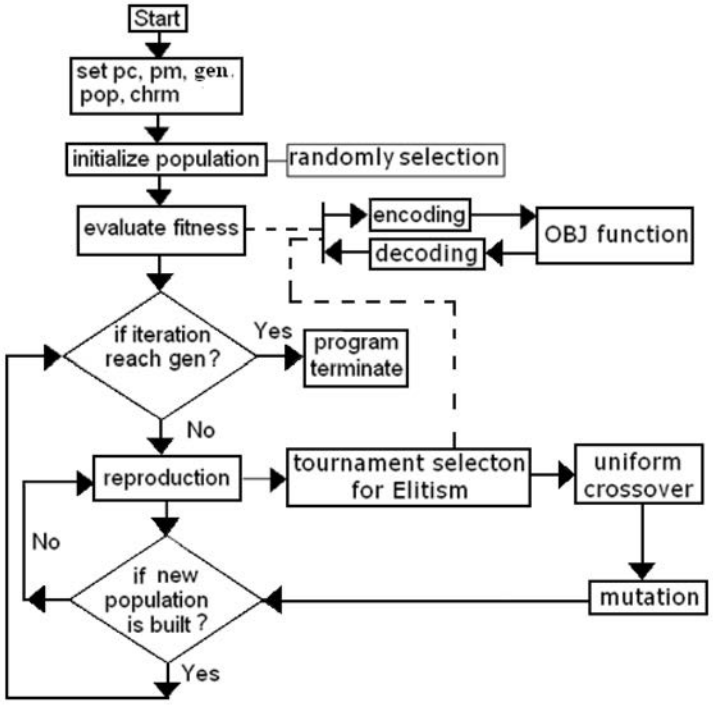

Fig. 7. The block diagram of the *GA* optimization on mufflers.

6. Results and discussion

6.1. Results

To achieve a good optimization, five kinds of *GA* parameters, including population size (*pop*), chromosome length (*chrm*), maximum generation (*gen*), crossover ratio (*pc*), and mutation ratio (*pm*), are varied step by step during optimization. The optimization system is encoded by Fortran and run on an IBM PC – Pentium IV. The results of two kinds of optimizations, one pure tone noise and the other broadband noise, are described as follows:

A. Pure Tones Noise Optimization

Twelve sets of *GA* parameters are tested by varying the values of the *GA* parameters. The simulated results with respect to the pure tone of 500 Hz are summarized and shown in Table 3. As indicated in Table 3, the optimal design

Table 3. Comparison of the results for the variations of control parameters – *pop, gen, chrm, pc, pm, elt* for muffler C [targeted pure tone of 500 Hz].

Item	GA parameters						Results				
	pop	*gen*	*chrm*	*pc*	*pm*	*elt*					
1	2	3	4	5	6	7	8	9	10	11	12
1	80	10	10	0.3	0.03	1	RT_1	RT_2	RT_3	RT_4	STL_{500}
							0.7939	0.2585	0.2457	0.2264	42.4
							RT_5	RT_6	RT_7	RT_8	
							0.3448	11191.0	0.0467	0.0037	
2	80	10	10	0.3	**0.05**	1	RT_1	RT_2	RT_3	RT_4	STL_{500}
							0.6839	0.3352	0.2562	0.2335	68.4
							RT_5	RT_6	RT_7	RT_8	
							0.2131	10491.7	0.0730	0.0061	
3	80	10	10	0.3	0.07	1	RT_1	RT_2	RT_3	RT_4	STL_{500}
							0.4132	0.6263	0.4851	0.3436	54.7
							RT_5	RT_6	RT_7	RT_8	
							0.6298	9952.9	0.0457	0.0033	
4	80	10	10	0.6	0.05	1	RT_1	RT_2	RT_3	RT_4	STL_{500}
							0.7917	0.5207	0.2489	0.2172	75.8
							RT_5	RT_6	RT_7	RT_8	
							0.3063	7253.6	0.0374	0.0051	
5	80	10	10	**0.9**	0.05	1	RT_1	RT_2	RT_3	RT_4	STL_{500}
							0.4963	0.6182	0.2637	0.2265	81.7
							RT_5	RT_6	RT_7	RT_8	
							0.3099	9706.3	0.0764	0.0028	

1	2	3	4	5	6	7	8	9	10	11	12
6	80	10	15	0.9	0.05	1	RT_1	RT_2	RT_3	RT_4	STL_{500}
							0.4368	0.5819	0.2741	0.2077	85.0
							RT_5	RT_6	RT_7	RT_8	
							0.2383	9382.7	0.0442	0.0062	
7	80	10	**20**	0.9	0.05	1	RT_1	RT_2	RT_3	RT_4	STL_{500}
							0.6531	0.6376	0.2467	0.2132	94.3
							RT_5	RT_6	RT_7	RT_8	
							0.2928	11197.0	0.0357	0.0051	
8	100	10	20	0.9	0.05	1	RT_1	RT_2	RT_3	RT_4	STL_{500}
							0.7369	0.6148	0.3263	0.2184	98.6
							RT_5	RT_6	RT_7	RT_8	
							0.3114	11440.9	0.0454	0.0055	
9	**120**	10	20	0.9	0.05	1	RT_1	RT_2	RT_3	RT_4	STL_{500}
							0.7261	0.5981	0.2445	0.2499	108.2
							RT_5	RT_6	RT_7	RT_8	
							0.4622	10726.3	0.0301	0.0026	
10	120	40	20	0.9	0.05	1	RT_1	RT_2	RT_3	RT_4	STL_{500}
							0.7431	0.5771	0.2537	0.2094	114.8
							RT_5	RT_6	RT_7	RT_8	
							0.2346	9694.9	0.0366	0.0040	
11	120	80	20	0.9	0.05	1	RT_1	RT_2	RT_3	RT_4	STL_{500}
							0.7779	0.6147	0.2450	0.2329	128.1
							RT_5	RT_6	RT_7	RT_8	
							0.4620	11321.7	0.0302	0.0056	
12	120	**160**	20	0.9	0.05	1	RT_1	RT_2	RT_3	RT_4	STL_{500}
							0.6558	0.5420	0.2437	0.2183	136.8
							RT_5	RT_6	RT_7	RT_8	
							0.2692	11324.0	0.0638	0.0029	

data can be obtained from the last set of *GA* parameters at (*pop, gen, chrm, pc, pm, elt*) = (120, 160, 20, 0.9, 0.05, 1). The *STL*-frequency profiles for the twelve sets are plotted in Figs. 8 and 9. As indicated in Fig. 9, the optimal *STL* is located at the target tone ($f = 500$ Hz). By using this *GA* parameter set with a pure tone of 800 Hz, the optimal muffler's design data with respect to various pure tones are obtained and summarized in Table 4. Using the optimal design in a theoretical calculation, two kinds of resultant curves of the *STL* with respect to frequencies are plotted and depicted in Fig. 10. As revealed in Fig. 10, the *STL*s are maximized at the desired frequencies.

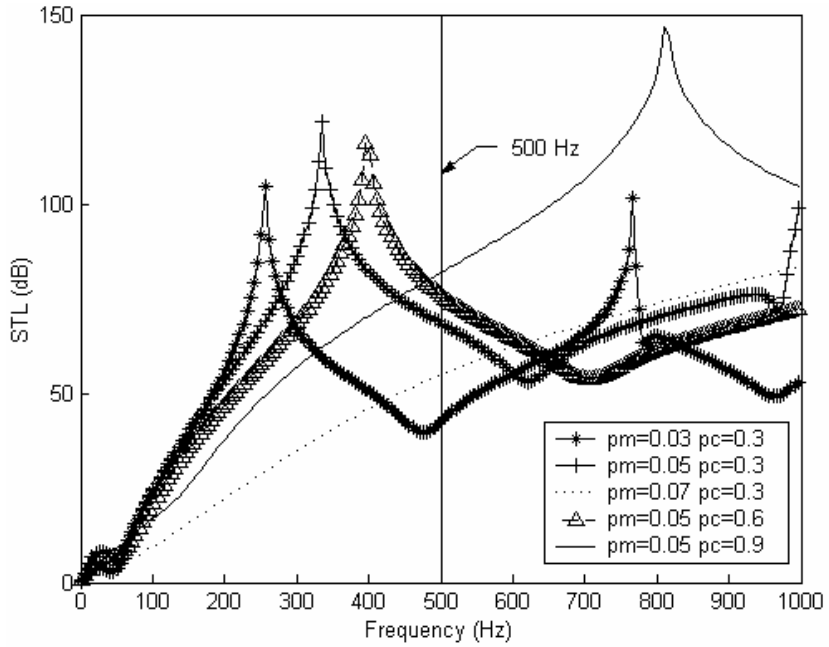

Fig. 8. The *STL* with respect to frequency for muffler C at the targeted tone of 500 Hz ($pop = 80$; $gen = 10$; $chrm = 10$; $elt = 1$).

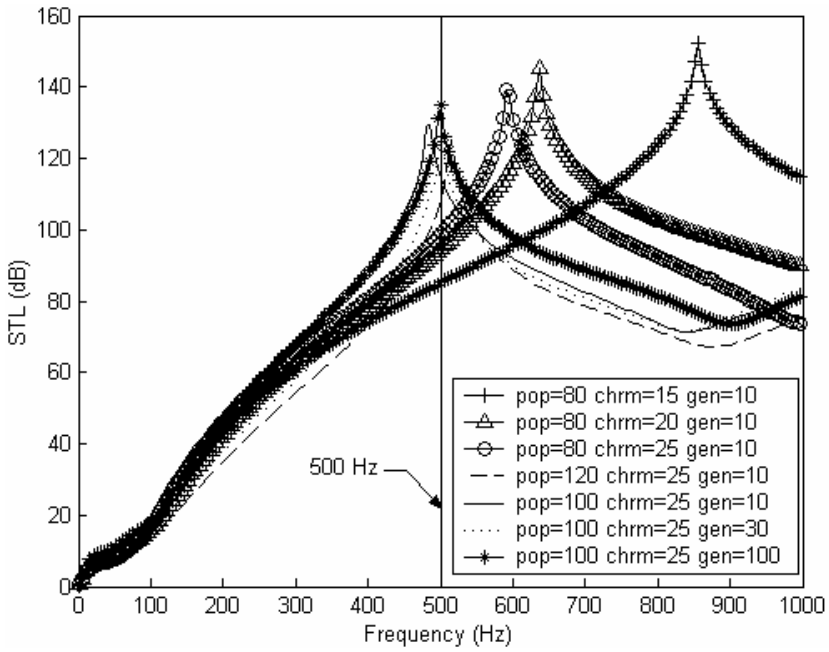

Fig. 9. The *STL* with respect to frequency for muffler C at the targeted tone of 500 Hz ($pc = 0.9$; $pm = 0.05$; $elt = 1$).

Table 4. Optimal design data with respect to various target frequencies for muffler C (targeted tones: 500 Hz, 800 Hz) ($pop = 120$; $gen = 160$; $chrm = 20$; $pc = 0.9$; $pm = 0.05$; $elt = 1$).

Target tones (Hz)	Results				
500	RT_1	RT_2	RT_3	RT_4	STL_{500}
	0.6558	0.5420	0.2437	0.2183	136.8
	RT_5	RT_6	RT_7	RT_8	
	0.2692	11324.0	0.0638	0.0029	
800	RT_1	RT_2	RT_3	RT_4	STL_{800}
	0.7875	0.7482	0.2731	0.2488	156.0
	RT_5	RT_6	RT_7	RT_8	
	0.2177	11656.0	0.0632	0.0066	

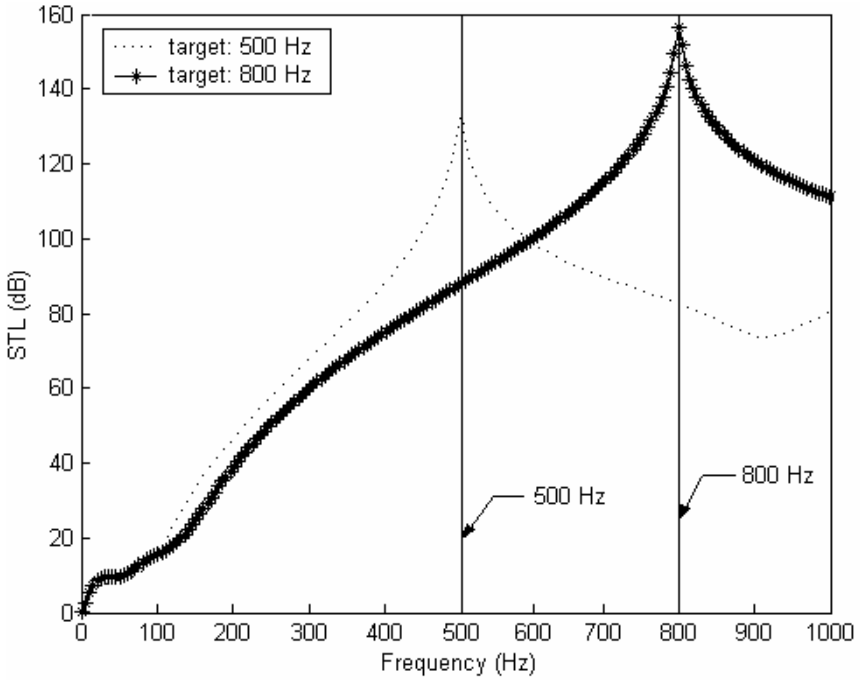

Fig. 10. Two kinds of resultant curves of the *STL* with respect to various targeted tones (500 and 800 Hz).

B. Broadband Noise Optimization

By using *GA* parameters at (*pop, gen, chrm, pc, pm, elt*) of (120, 160, 20, 0.9, 0.05, 1) in Eqs. (24), (26), (28), the optimal muffler's design parameters and size in minimizing the sound power level at the muffler's outlet are summarized in Table 5. As illustrated in Table 5, the resultant sound power level for mufflers A–C has been reduced from 138.9 dB(A) to 99.1, 123.5, and 84.5 dB(A). Using this

Table 5. Optimal design data for three kinds of mufflers (broadband noise) ($pop = 120$; $gen = 160$; $chrm = 20$; $pc = 0.9$; $pm = 0.05$; $elt = 1$).

Muffler types	Design parameters								Performance
Muffler A	RT_1^*	RT_2^*	RT_3^*	RT_4^*					SWL_T (dB)
	0.5340	0.5246	0.7079	0.2028					99.1
Muffler B	RT_1^{**}	RT_2^{**}	RT_3^{**}	RT_4^{**}	RT_5^{**}				SWL_T (dB)
	0.3736	6315.0	0.003269	0.05025	0.5157				123.5
Muffler C	RT_1	RT_2	RT_3	RT_4	RT_5	RT_6	RT_7	RT_8	SWL_T (dB)
	0.6987	0.2281	0.4848	0.2056	0.2084	4526.5	0.0851	0.0029	84.5

optimal design in a theoretical calculation, the resultant curve of the SWL with respect to those frequencies is plotted and depicted in Fig. 11. As revealed in Fig. 11, the original sound power level ($SWLO$) can be reduced to appropriate spectrum characteristics.

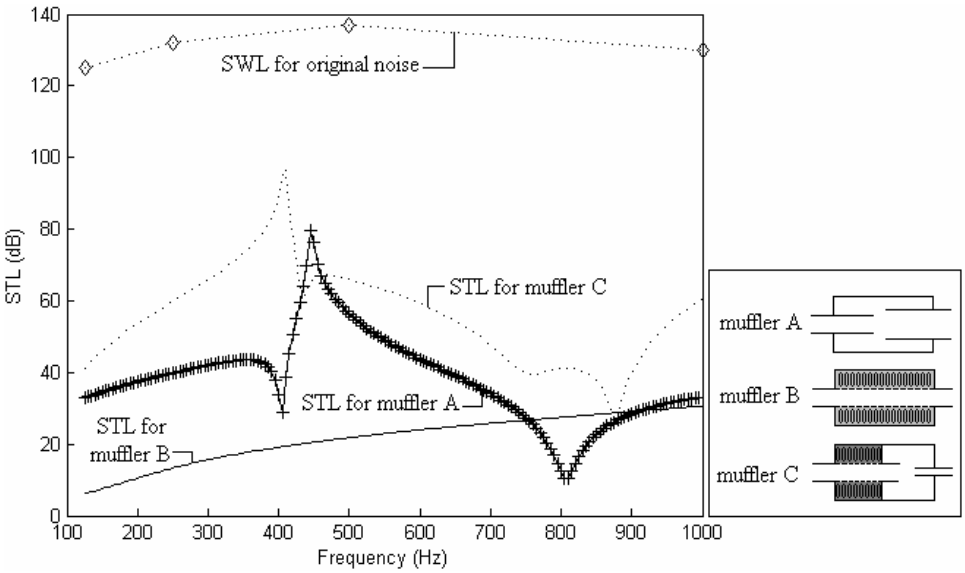

Fig. 11. Comparison of STLs with respect to the original sound power level ($SWLO$) in a frequency's domain.

6.2. Discussion

To achieve a better and sufficient optimization, the selection of the appropriate GA parameters set is essential. As indicated in Table 3, the twelve GA sets are better solutions with respect to the optimization of pure tone noise at 500 Hz. The optimal design data with respect to various pure tones are illustrated in Ta-

ble 4 and Fig. 10. By adjusting the muffler shapes, eight design parameters play essential roles in tuning the *STL*'s peak to the desired frequency. As indicated in Fig. 10, the predicted maximal values of *STL*, an acoustical performance, are precisely located at the desired frequency. Moreover, the *GA*'s solution for the broadband noise is shown in Table 5 and Fig. 11. As indicated in Table 5, the overall sound transmission losses for mufflers A–C (muffler A: reactive muffler; muffler B: dissipative muffler; muffler C: hybrid muffler) reach 39.8, 15.4, and 54.4 dB. As can be observed in Fig. 11, muffler A has better noise elimination at a lower frequency; on the other hand, muffler B has excellent noise reduction at a higher frequency. However, for the gas-venting noise, the noise levels in both the lower band and the higher band frequencies are strong enough. Here, it is obvious that muffler C, having both the reactive chamber and dissipative chamber, is superior to the other two mufflers.

7. Conclusion

It has been shown that mufflers in conjunction with a *GA* optimizer can be easily optimized under space limits by using a numerical decoupling technique, plane wave theory, as well as a four-pole transfer matrix. As indicated in Table 3 and Figs. 8, 9, twelve kinds of *GA* parameters (*pop, gen, chrm, pc, pm, elt*) play essential roles in the solution's accuracy during *GA* optimization. As indicated in Fig. 10, the *STL* is precisely maximized at the desired frequency; therefore, the tuning ability established by adjusting the design parameters of the mufflers is reliable. As indicated in Fig. 11, muffler A, having a narrow-band *STL* in lower frequencies, will be suitable for eliminating the pure tone and lower frequency noise. However, muffler B has better noise reduction at higher frequencies. In dealing with a broadband higher frequency noise, mufflers A and B are insufficient. It has been seen that the overall acoustical performance will be substantially improved using muffler C where both the reactive chamber and the dissipative chamber are hybridized. Consequently, muffler C, having hybrid chambers (a reactive chamber and a dissipative chamber) resulting in the widest band and highest *STL* in both lower and higher frequency, is superior to mufflers A and B. This approach used for the optimal design of the *STL* proposed in this study is quite effective.

Appendix. Transfer Matrix of a Perforated Chamber Filled with a Sound Absorbing Wool

As indicated in Fig. 12, the perforated resonator is composed of an inner perforated tube and an outer resonating chamber. Based on Sullivan and Crocker's derivation (1978), the continuity equations and momentum equations with respect to inner and outer tubes at nodes 1 and 2 are listed below.

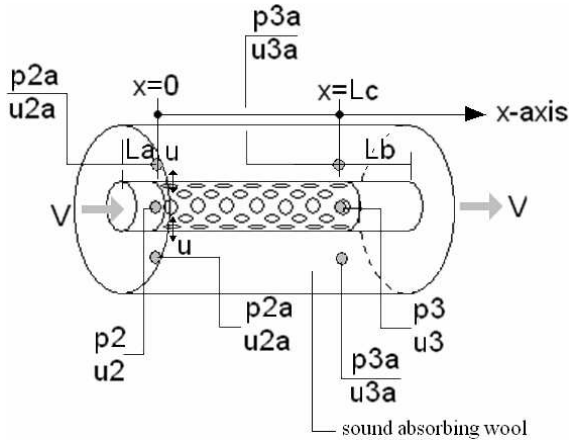

Fig. 12. Acoustic field of a dissipative chamber.

Inner tube:

– continuity equation:

$$V\frac{\partial \rho_2}{\partial x} + \rho_o \frac{\partial u_2}{\partial x} + \frac{4\rho_o}{D_1}u + \frac{\partial \rho_2}{\partial t} = 0, \tag{A1}$$

– momentum equation:

$$\rho_o \left(\frac{\partial}{\partial t} + V\frac{\partial}{\partial x}\right) u_2 + \frac{\partial p_2}{\partial x} = 0. \tag{A2}$$

Outer tube:

– continuity equation:

$$\widetilde{\rho}\frac{\partial u_{2a}}{\partial x} - \frac{4D_1\widetilde{\rho}}{D_o^2 - D_1^2}u + \frac{\partial \rho_{2a}}{\partial t} = 0, \tag{A3}$$

– momentum equation:

$$\widetilde{\rho}\frac{\partial u_{2a}}{\partial t} + \frac{\partial p_{2a}}{\partial x} = 0. \tag{A4}$$

Assuming that the acoustic wave is a harmonic motion

$$p(x,t) = P(x)\cdot e^{j\omega t}, \tag{A5}$$

under the isentropic processes in ducts, it yields

$$P(x) = \rho(x)\cdot c_o^2. \tag{A6}$$

Assuming that the perforation along the inner tube is uniform ($d\varsigma/dx = 0$), the acoustic impedance of the perforation ($\rho_o c_o \varsigma$) is

$$\rho_o c_o \zeta = \frac{p_2(x) - p_{2A}(x)}{u(x)}, \tag{A7}$$

where ς is the specific acoustical impedance of the perforated tube.

The empirical formulations developed by Sullivan and Crocker (1978) and Rao (1984) for the perforates with and without mean flow are adopted in this study.

For perforates with a stationary medium, we have

$$\xi_{1A} = [0.006 + jk(t + 0.75dh_{1A})]/\eta_{1A}. \tag{A8)$_1$}$$

For perforates with a grazing flow, we have

$$\xi_{1A} = [0.514d_1M_1/(L_{C1A}\eta_{1A}) + j0.95k(t + 0.75dh_{1A})]/\eta_{1A}, \tag{A8)$_2$}$$

where dh_{1A} is the diameter of a perforated hole on an inner tube, t is the thickness of an inner perforated tube, and $\eta$is the porosity of the perforated tube.

Plugging Eqs. (A5)–(A7) into Eqs. (A1)–(A4) and eliminating u_1 and u_2, we have

$$\left[\left(1 - M^2\right)\frac{\mathrm{d}^2}{\mathrm{d}x^2} - 2jMk\frac{\mathrm{d}}{\mathrm{d}x} + k^2\right]p_2 - \frac{4}{D_1\varsigma}\left[M\frac{\mathrm{d}}{\mathrm{d}x} + jk\right](p_2 - p_{2a}) = 0, \tag{A9}$$

$$\left[\frac{\mathrm{d}^2}{\mathrm{d}x^2} + \widetilde{k}^2\right]p_{2a} + j\frac{4kD_1\widetilde{\rho}}{(D_o^2 - D_1^2)\varsigma\rho_0}(p_2 - p_{2a}) = 0, \tag{A10}$$

where $M_2 = \dfrac{V_2}{c_o}$.

Alternatively, Eqs. (A9) and (A10) can be expressed as

$$p_2'' + \alpha_1 p_2' + \alpha_2 p_2 + \alpha_3 p_{2A}' + \alpha_4 p_{2A} = 0, \tag{A11)$_1$}$$

$$\alpha_5 p_2' + \alpha_6 p_2 + p_{2A}'' + \alpha_7 p_{2A}' + \alpha_8 p_{2A} = 0, \tag{A11)$_2$}$$

where

$$\alpha_1 = -\frac{jM}{1 - M^2}\left(2k - j\frac{4}{D_1\varsigma}\right); \qquad \alpha_2 = \frac{1}{1 - M^2}\left(k^2 - j\frac{4k}{D_1\varsigma}\right);$$

$$\alpha_3 = \frac{M}{1 - M^2}\cdot\frac{4}{D_1\varsigma}; \qquad \alpha_4 = \frac{j}{1 - M^2}\cdot\frac{4k}{D_1\varsigma};$$

$$\alpha_5 = 0; \qquad \alpha_6 = \frac{j4kD_1\widetilde{\rho}}{(D_o^2 - D_1^2)\varsigma\rho_o}; \tag{A11)$_3$}$$

$$\alpha_7 = 0; \qquad \alpha_8 = \widetilde{k}^2 - \frac{j4kD_1\widetilde{\rho}}{(D_o^2 - D_1^2)\varsigma\rho_o};$$

$$k = \frac{\omega}{c}.$$

Let

$$p_2' = \frac{\mathrm{d}p_2}{\mathrm{d}x} = y_1, \qquad p_{2A}' = \frac{\mathrm{d}p_{2A}}{\mathrm{d}x} = y_2, \qquad p_2 = y_3, \qquad p_{2A} = y_4. \tag{A12}$$

According to Eqs. (A11) and (A12), the new matrix between $\{y'\}$ and $\{y\}$ is

$$\begin{bmatrix} y_1' \\ y_2' \\ y_3' \\ y_4' \end{bmatrix} = \begin{bmatrix} -\alpha_1 & -\alpha_3 & -\alpha_2 & -\alpha_4 \\ -\alpha_5 & -\alpha_7 & -\alpha_6 & -\alpha_8 \\ 1 & 0 & 0 & 0 \\ 0 & 1 & 0 & 0 \end{bmatrix} \begin{bmatrix} y_1 \\ y_2 \\ y_3 \\ y_4 \end{bmatrix} \tag{A13}_1$$

which can be briefly expressed as

$$\{y'\} = [\mathrm{N}]\,\{y\}. \tag{A13}_2$$

Let

$$\{y\} = [\Omega]\,\{\Gamma\} \tag{A14}_1$$

which is

$$\begin{bmatrix} \mathrm{d}p_2/\,\mathrm{d}x \\ \mathrm{d}p_{2A}/\,\mathrm{d}x \\ p_2 \\ p_{2A} \end{bmatrix} = \begin{bmatrix} \Omega_{1,1} & \Omega_{1,2} & \Omega_{1,3} & \Omega_{1,4} \\ \Omega_{2,1} & \Omega_{2,2} & \Omega_{2,3} & \Omega_{2,4} \\ \Omega_{3,1} & \Omega_{3,2} & \Omega_{3,3} & \Omega_{3,4} \\ \Omega_{4,1} & \Omega_{4,2} & \Omega_{4,3} & \Omega_{4,4} \end{bmatrix} \begin{bmatrix} \Gamma_1 \\ \Gamma_2 \\ \Gamma_3 \\ \Gamma_4 \end{bmatrix}, \tag{A14}_2$$

$[\Omega]_{4\times4}$ is the model matrix formed by four sets of eigen vectors $\Omega_{4\times1}$ of $[\mathrm{N}]_{4\times4}$.

Combining Eq. (A14) with (A13) and then multiplying $[\Omega]^{-1}$ by both sides yield

$$[\Omega]^{-1}[\Omega]\{\Gamma'\} = [\Omega]^{-1}[\mathrm{N}][\Omega]\{\Gamma\}.$$

Set

$$[\chi] = [\Omega]^{-1}[\mathrm{N}][\Omega] = \begin{bmatrix} r_1 & 0 & 0 & 0 \\ 0 & r_2 & 0 & 0 \\ 0 & 0 & r_3 & 0 \\ 0 & 0 & 0 & r_4 \end{bmatrix}, \tag{A15}$$

where r_i is the eigen value of [N].

Equation (A13) can be thus rewritten as

$$\{\Gamma'\} = [\chi]\,\{\Gamma\}. \tag{A16}$$

Obviously, Eq. (A15) is a decoupled equation. The related solution obtained is

$$\Gamma_i = C_i e^{r_i x}. \tag{A17}$$

Plugging Eq. (A17) into $(\mathrm{A14})_2$ and rearranging them, we have

$$\begin{bmatrix} p_2(x) \\ p_{2a(x)} \\ \dfrac{\mathrm{d}p_2(x)}{\mathrm{d}x} \\ \dfrac{\mathrm{d}p_{2a}(x)}{\mathrm{d}x} \end{bmatrix} = \begin{bmatrix} \Omega_{3,1}e^{r_1x} & \Omega_{3,2}e^{r_2x} & \Omega_{3,3}e^{r_3x} & \Omega_{3,4}e^{r_4x} \\ \Omega_{4,1}e^{r_1x} & \Omega_{4,2}e^{r_2x} & \Omega_{4,3}e^{r_3x} & \Omega_{4,4}e^{r_4x} \\ \Omega_{1,1}e^{r_1x} & \Omega_{1,2}e^{r_2x} & \Omega_{1,3}e^{r_3x} & \Omega_{1,4}e^{r_4x} \\ \Omega_{2,1}e^{r_1x} & \Omega_{2,2}e^{r_2x} & \Omega_{2,3}e^{r_3x} & \Omega_{2,4}e^{r_4x} \end{bmatrix} \begin{bmatrix} C_1 \\ C_2 \\ C_3 \\ C_4 \end{bmatrix}. \tag{A18}$$

From Eqs. (A2) and (A4), we have

$$\rho_o c_o u_2 = -\frac{1}{jk + M\gamma_i}\frac{\mathrm{d}p_2}{\mathrm{d}x}; \qquad \widetilde{\rho}\,\widetilde{c}u_{2a} = -\frac{1}{j\widetilde{k}}\frac{\mathrm{d}p_{2a}}{\mathrm{d}x}. \tag{A19}$$

Plugging Eq. (A19) into (A18) yields

$$\begin{bmatrix} p_2(x) \\ p_{2a}(x) \\ \rho_o c_o u_2(x) \\ \widetilde{\rho}\,\widetilde{c}u_{2a}(x) \end{bmatrix} = \begin{bmatrix} \mathrm{H}_{1,1} & \mathrm{H}_{1,2} & \mathrm{H}_{1,3} & \mathrm{H}_{1,4} \\ \mathrm{H}_{2,1} & \mathrm{H}_{2,2} & \mathrm{H}_{2,3} & \mathrm{H}_{2,4} \\ \mathrm{H}_{3,1} & \mathrm{H}_{3,2} & \mathrm{H}_{3,3} & \mathrm{H}_{3,4} \\ \mathrm{H}_{4,1} & \mathrm{H}_{4,2} & \mathrm{H}_{4,3} & \mathrm{H}_{4,4} \end{bmatrix} \begin{bmatrix} C_1 \\ C_2 \\ C_3 \\ C_4 \end{bmatrix}. \tag{A20}$$

Substituting two cases of $x = 0$ and $x = Lc$ into Eq. (A20) yields

$$\begin{bmatrix} p_2(0) \\ p_{2a}(0) \\ \rho_o c_o u_2(0) \\ \widetilde{\rho}\,\widetilde{c}u_{2a}(0) \end{bmatrix} = [\mathrm{A}] \begin{bmatrix} p_2(L_C) \\ p_{2a}(L_C) \\ \rho_o c_o u_2(L_C) \\ \widetilde{\rho}\,\widetilde{c}u_{2a}(L_C) \end{bmatrix}, \tag{A21}_1$$

where

$$[\mathrm{A}] = [\mathrm{H}(0)][\mathrm{H}(L_C)]^{-1}. \tag{A21}_2$$

The boundary conditions for the inner tube are

$$\frac{p_{2a}(0)}{-u_{2a}(0)} = -j\widetilde{\rho}\,\widetilde{c}\cot(\widetilde{k}L_A) \qquad \text{at } x = 0, \tag{A22}_1$$

$$\frac{p_{2a}(L_C)}{u_{2a}(L_C)} = -j\widetilde{\rho}\,\widetilde{c}\cot(\widetilde{k}L_B) \qquad \text{at } x = L_{C1A}. \tag{A22}_2$$

Plugging Eq. (A22) into (A21) yields

$$\begin{bmatrix} p_2(0) \\ \rho_o c_o u_2(0) \end{bmatrix} = \begin{bmatrix} TPD_{1,1} & TPD_{1,2} \\ TPD_{2,1} & TPD_{2,2} \end{bmatrix} \begin{bmatrix} p_{2A}(L_{C1A}) \\ \rho_o c_o u_{2A}(L_{C1A}) \end{bmatrix}. \tag{A23}_1$$

The simplified alternative form is

$$\begin{bmatrix} p_2 \\ \rho_o c_o u_2 \end{bmatrix} = \begin{bmatrix} TPD_{1,1} & TPD_{1,2} \\ TPD_{2,1} & TPD_{2,2} \end{bmatrix} \begin{bmatrix} p_3 \\ \rho_o c_o u_3 \end{bmatrix}, \tag{A23}_2$$

where

$$
\begin{aligned}
p_2 &= p_2(0),\\
u_2 &= u_2(0),\\
p_3 &= p_{2A}(L_{C1A}),\\
u_3 &= u_{2A}(L_{C1A}),\\
TP_{1,1} &= A_{1,1} + K_1K_2,\\
TP_{1,2} &= (A_{1,3} + N_1K_2),\\
TP_{2,1} &= (A_{3,1} + K_1N_2),\\
TP_{2,2} &= A_{3,3} + N_1N_2,\\
K_1 &= (Q_1A_{2,1} - A_{4,1})/R_1,\\
N_1 &= (Q_1A_{2,3} - A_{4,3})/R_1,\\
K_2 &= A_{1,2} + Q_2A_{1,4},\\
N_2 &= A_{3,2} + Q_2A_{3,4},\\
R_1 &= A_{4,2} + Q_2A_{4,4} + Q_1(A_{2,2} - Q_2A_{2,4}),\\
Q_1 &= -j\tan(\widetilde{k}L_A),\\
Q_2 &= +j\tan(\widetilde{k}L_B).
\end{aligned}
\qquad (\text{A23})_3
$$

According to Johnson *et al.* (1987), the effective density for the sound absorbing wool is expressed as

$$
\widetilde{\rho}(\omega) = \rho_o\alpha_\infty\left[1 + \frac{\sigma_{fr}\Omega}{j\alpha_\infty\rho_o\omega}\left(1 + \frac{4j\alpha_\infty^2\mu\rho_o\omega}{\sigma_{fr}^2 l_{cl}^2\Omega^2}\right)^{1/2}\right], \qquad (\text{A24})
$$

$$
l_{cl} = S\left(\frac{8\mu\alpha_\infty}{\sigma_{fr}\Omega}\right)^{1/2}, \qquad (\text{A25})
$$

where μ is the viscosity for the air, α_∞ is the structure factor for the wool, Ω is porosity for the wool, σ_{fr} is the flowing resistance for the wool, l_{cl} is the characteristic length, and S^2 is within 0.1–10.

Subsequently, according to Allard and Champoux (1992), the dynamic bulk modulus $K(\omega)$ for porous wool is

$$K(\omega)=\gamma P_0\left\{\gamma-\frac{\gamma-1}{\left[1+\dfrac{\varsigma'_{fr}\Omega}{j\alpha_\infty\rho_o N_{pr}\omega}\left(1+\dfrac{4j\alpha_\infty^2\mu\rho_o N_{pr}\omega}{\sigma'^2_{fr}l'^2_{cl}\Omega^2}\right)^{1/2}\right]}\right\}^{-1}, \quad (A26)_1$$

$$l'_{cl}=\left(\frac{8\mu\alpha_\infty}{\sigma'_{fr}\Omega}\right)^{1/2}, \quad (A26)_2$$

where γ is the specific heat, P_0 is the pressure in atmosphere, N_{pr} is the Prandtl number, and l'_{cl} is a new characteristic length.

$\widetilde{k}(\omega)$, the wave number for the wool, is expressed as the density $\widetilde{\rho}(\omega)$ and the dynamic bulk modulus $K(\omega)$.

$$\widetilde{k}(\omega)=\omega\left[\frac{\widetilde{\rho}\,(\omega)}{K\,(\omega)}\right]^{1/2}. \quad (A27)$$

Moreover, $\widetilde{c}$, the sound speed in the wool, is (Selamet *et al.*, 2001; Xu *et al.*, 2004)

$$\widetilde{c}=\frac{c_o}{\mathrm{Re}\,al\left(\frac{\widetilde{k}}{k_o}\right)}. \quad (A28)$$

Acknowledgments

The author acknowledges the financial support of the National Science Council (NSC99-2221-E-235-001, Taiwan, ROC) and would also like to thank the anonymous referees who kindly provided the suggestions and comments to improve this work.

References

1. Allard J.F., Champoux Y. (1992), *New empirical equations for sound propagation in rigid frame fibrous materials*, J. Acoust. Soc. Am., **41**, 3346–3353.
2. Chiu M.C. (2009), *SA optimization on multi-chamber mufflers hybridized with perforated plug-inlet under space constraints*, Archives of Acoustics, **34**, 3, 305–343.
3. Chiu M.C., Chang Y.C., Yeh L.J. (2008), *Numerical assessment of optimal one-chamber perforated mufflers by using GA method*, Material Science Forum, **594**, 368–376.
4. Cummings A., Chang I.J. (1987), *Internal mean flow effects on the characteristics of bulk-reacting liners in circular ducts*, Acustica, **64**, 169–178.

5. Cummings A., Chang I.J. (1988), *Sound attenuation of a finite length dissipative flow duct silencer with internal mean flow in the absorbent*, Journal of Sound and Vibration, **127**, 1–17.

6. Glav R. (2000), *The transfer matrix for a dissipative silencer of arbitrary cross-section*, Journal of Sound and Vibration, **236**, 575–594.

7. Holland J. (1975), *Adaptation in Natural and Artificial System*, Ann Arbor, University of Michigan Press.

8. Jayaraman K., Yam K. (1981), *Decoupling approach to modeling perforated tube muffler component*, J. Acous. Soc. Am., **69**, 2, 390–396.

9. Johnson D.L., Koplik J., Dashen R. (1987), *Theory of dynamic permeability and tortuosity in fluid saturated porous media*, J. Fluid Mech., **176**, 379–402.

10. Jong D. (1975), *An Analysis of the Behavior of a Class of Genetic Adaptive Systems*, Doctoral Thesis, Department of Computer and Communication Sciences, Ann Arbor, University of Michigan.

11. Ko S.H. (1975), *Theoretical analyses of sound attenuation in acoustically lined flow ducts separated by porous splitters (rectangular, annular and circular ducts)*, Journal of Sound and Vibration, **39**, 471–487.

12. Lee I.J. (2005), *Acoustic Characteristics of Perforated Dissipative and Hybrid Silencers*, Doctor thesis, Ohio State University.

13. Morse P.M. (1939), *Transmission of sound inside pipes*, J. Acoust. Soc. Am., **11**, 205–210.

14. Munjal M.L. (1987), *Acoustics of Ducts and Mufflers with Application to Exhaust and-Ventilation System Design*, John Wiley and Sons, New York.

15. Munjal M.L. (2003), *Analysis and design of pod silencers*, Journal of Sound and Vibration, **262**, 497–507.

16. Munjal M.L., Rao K.N., Sahasrabudhe A.D. (1987), *Aeroacoustic analysis of perforated muffler components*, Journal of Sound and Vibration, **114**, 2, 173–188.

17. Peat K.S. (1988), *A numerical decoupling analysis of perforated pipe silencer elements*, Journal of Sound and Vibration, **123**, 2, 199–212.

18. Peat K.S. (1991), *A transfer-matrix for an absorption silencer element*, Journal of Sound and Vibration, **146**, 353–360.

19. Rao K.N., Munjal M.L. (1984), *A generalized decoupling method for analyzing perforated element mufflers*, Nelson Acoustics Conference, Madison.

20. Scott R.A. (1946), *The propagation of sound between walls of porous material*, Proceedings of the Physical Society, **58**, 358–368.

21. Selamet A., Lee I.J., Huff N.T. (2003), *Acoustic attenuation of hybrid silencers*, Journal of Sound and Vibration, **262**, 509–527.

22. Selamet A., Lee I.J., Ji Z.L., Huff N.T. (2001), *Acoustic attenuation performance of perforated concentric absorbing silencers*, SAE Noise and Vibration Conference and Exposition, SAE Paper No. 2001-01-1435, Traverse City, MI, April 30 – May 3.

23. Sullivan J.W. (1979), *A method of modeling perforated tube muffler components I: theory*, J. Acous, Soc. Am., **66**, 772–778.

24. Sullivan J.W. (1979), *A method of modeling perforated tube muffler components II: theory*, J. Acous. Soc. Am., **66**, 779–788.

25. Sullivan J.W., Crocker M.J. (1978), *Analysis of concentric tube resonators having unpartitioned cavities*, J. Acous. Soc. Am., **64**, 207–215.

26. Thawani P.T., Jayaraman K. (1983), *Modeling and applications of straight-through resonators*, J. Acous. Soc. Am., **73**, 4, 1387–1389.

27. Wang C.N. (1992), *The Application of Boundary Element Method in the Noise Reduction Analysis for the Automotive Mufflers*, Doctor thesis, Taiwan University.

28. Wang C.N., Hsieh C.C. (2000), *Experimental study for muffler components with flow*, Bulletin of the College of Engineering, N.T.U., **78**, 67–74.

29. Xu M.L., Selamet A., Lee I.J., Huff N.T. (2004), *Sound attenuation in dissipative expansion chambers*, Journal of Sound and Vibration, **272**, 1125–1133.